AERODYNAMIC INTERFERENCE CHARACTERISTICS OF BUSEMANN BIPLANE AIRFOIL WITH SLAT AND FLAP IN LOW-SPEED FLOW

Thai Duong Nguyen[1,*], Quang Huy Pham[2], The Hung Tran[3]
[1]*Vietnam-Japan International Cooperation Center for Science and Technology, Le Quy Don Technical University*
[2]*Unmanned Aerial Vehicles Center, Viettel Hi-Technology Industries Corporations*
[3]*Faculty of Aerospace Engineering, Le Quy Don Technical University*

Abstract

In this study, aerodynamic interference characteristics of a Busemann biplane incorporating both leading-edge slats and trailing-edge flaps are investigated, utilizing wind tunnel experiments and numerical simulations. The aerodynamic characteristics of the biplane configuration are assessed through a comparative analysis with the performances of its individual upper and lower wings when operating as single configurations. The deflections of the slat and flap are 15° and 30°, respectively. Stall occurred on both the upper and lower wings in the single configuration. The addition of the leading-edge slat enabled the single model to stall at a larger angle of attack, consequently leading to a higher maximum lift coefficient. In the biplane configuration with slat and flap, the lower wing did not experience stall, and its lift coefficient increased with the angle of attack, similar to the case with only trailing-edge flaps. The drag interference ratio was observed to exceed 1.0 at angles of attack below 5° for the biplane with only a trailing-edge flap and below 12° for the configuration including both a slat and a flap. This finding implies that, within these ranges, the biplane generated a higher total drag compared to the sum of the individual drag values of each element in a single-element configuration. The lift interference ratio exhibited a minimum value of 0.72 at 16° for the biplane with both slat and flap.

Keywords: *Busemann biplane; leading-edge slat; trailing-edge flap; interference ratio.*

1. Introduction

Mitigation of the sonic boom remains a critical challenge in the advancement of next-generation supersonic transport (SST). The Busemann biplane concept, investigated by Tohoku University in Japan, has attracted significant interest for its potential application in next-generation supersonic transport aircraft [1], [2]. The Busemann biplane airfoil is characterized by a unique configuration wherein the inter-wing spacing is calculated to cancel the shock wave between the upper and lower elements at supersonic regimes. This arrangement offers the potential for significant reductions in

[*] Corresponding author, email: duongnt@lqdtu.edu.vn
DOI: 10.56651/lqdtu.jst.v21.n1.995

sonic boom and aerodynamic drag. Kusunose *et al.* demonstrated that the Busemann biplane can reduce wave drag by over 80% compared to a diamond-shaped wing of the same wing thickness at the design Mach number ($M\infty = 1.7$) [1], [2]. Furthermore, the peak pressure value near the Busemann biplane is significantly reduced, mitigating the sonic boom transmitted to the ground. This value is only about 1/10 of that of the Concorde during cruise flight, demonstrating the potential application of the Busemann biplane in the development of next-generation supersonic aircraft. Moreover, previous experimental and numerical investigations have been conducted to elucidate the aerodynamic characteristics and interference phenomena in these configurations at supersonic speeds [3], [4]. In addition, the 3D wing models and wing-body models have been proposed with promising research results [5]-[8].

Previous investigations point out that the Busemann wing shows the low performance at off-design operational conditions [1], [2]. Therefore, the integration of leading-edge slats and trailing-edge flaps has been explored to improve the wing aerodynamic performances. In addition to mitigating flow choking and hysteresis, using these control surfaces clearly improves aerodynamic efficiency in the low-speed flight regime. In previous research, Maruyama *et al.* [9] proposed the utilization of leading-edge slats and trailing-edge flaps at low-speed flows, with an achieved total lift coefficient of 2.025 in a specific configuration, meeting the requirements for takeoff and landing. Kashitani *et al.* [10] also conducted wind tunnel experiments on a baseline model, with the flow field analyzed using a smoke-flow visualization system. However, as the angle of attack increased, significant discrepancies were observed in the results due to flow instabilities and the influence of large vortices.

Nguyen *et al.* [11] analyzed a Busemann airfoil and a staggered configuration by wind tunnel experiments and numerical simulations. The results focused on the aerodynamic coefficients and interference between the upper and lower elements. The aerodynamic interference of the Buseman biplane was quantitatively investigated and compared with the upper and lower wings in single configurations. In a biplane configuration, the upper wing produced less drag and lift than a single wing when the angle of attack was above 5º. When the angle of attack exceeded 20º, the upper wing generated negligible lift within the biplane setup.

Several investigations showed that a 30º trailing-edge flap enhances the maximum total lift coefficient of the Busemann biplane airfoil from 1.6 to 2.15 at an angle of attack of 7º [12], [13]. Furthermore, a 15º leading-edge slats mitigate flow separation across the surfaces of both the upper and lower wings, thereby reducing drag relative to configurations employing only trailing-edge flaps. Based on previous studies, a

configuration with 30º flap is recommended for takeoff, while 15º slat and 30º flap are advised for landing. However, the aerodynamic interference phenomena of a Busemann biplane incorporating both slats and flaps remain unclear. Consequently, further comprehensive research is necessary to elucidate the specific aerodynamic characteristics and performances of biplane configurations when installed slats and flaps.

This study investigates the aerodynamic interference phenomena exhibited by a Busemann biplane airfoil incorporating both leading-edge slats and trailing-edge flaps within a low-speed flow regime, utilizing wind tunnel experiments and numerical simulations. The aerodynamic characteristics of the biplane configuration are assessed through a comparative analysis with the performances of its individual upper and lower wings when operating as single-wing configurations.

2. Experimental setup

2.1. Wind tunnel and balance systems

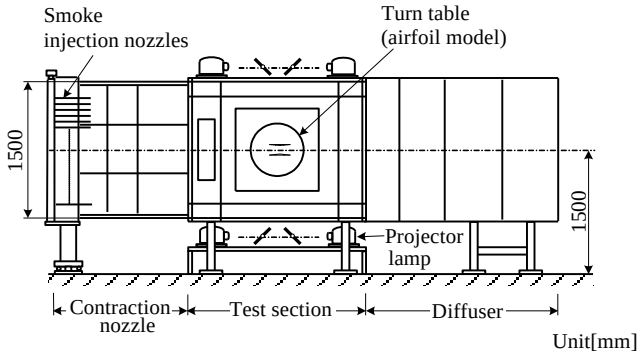

(a) Low-speed wind tunnel system (Side view)

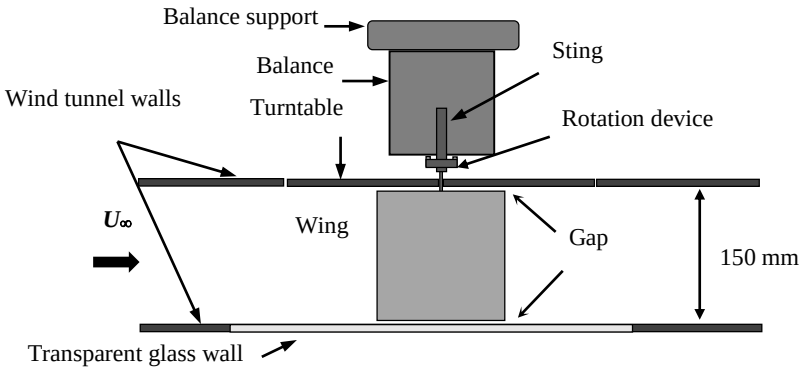

*(b) The force balance system*s

Fig. 1. Low-speed wind tunnel system [11].

The experiments were conducted using a low-speed wind tunnel system, with a maximum flow velocity of 26 m/s. Figure 1 [11] shows an overview of the wind tunnel system. The test section has dimensions of length × width × height of 2500 mm × 150 mm × 1500 mm. The wall of the test section is designed with a circular turntable to fix and adjust the angle of attack of the model. The position of the turntable is located in the middle of the wall, with the center of the circular turntable at a height of 750 mm from the base of the chamber wall.

The force balance system is mounted on the side wall of the test section. The angle of attack of the model is adjusted using both a turntable and a rotating device on the force balance. The wind tunnel system, force balance, and design have been thoroughly described in previous studies [11], [12].

2.2. Experimental models

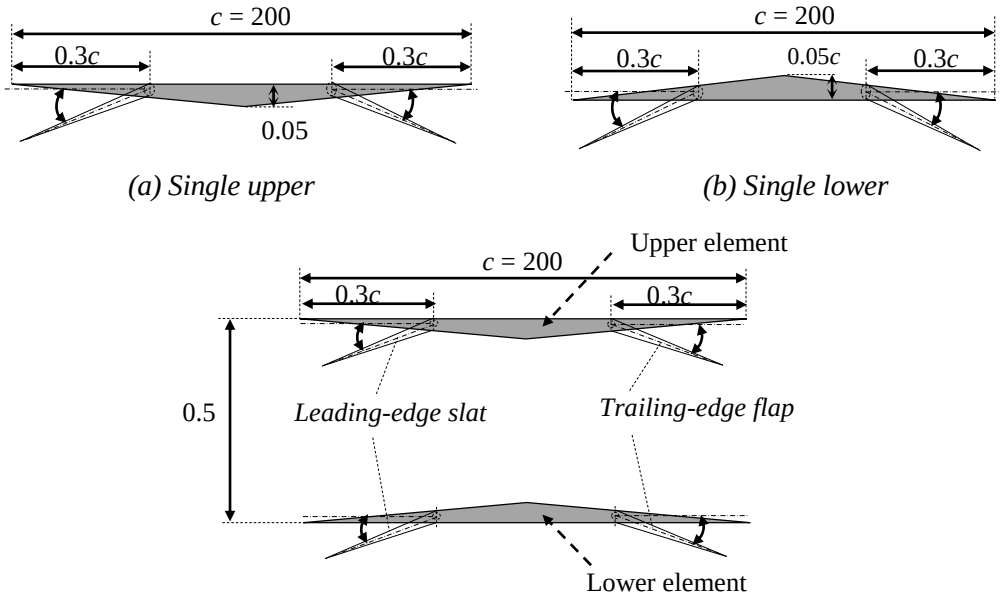

(a) Single upper *(b) Single lower*

(c) Biplane model

Fig. 2. Experimental model configurations.

Figure 2 shows an overview of the experimental models. Figs. 2(a) and 2(b) show the single upper and lower element model combined with slat and flap. Fig. 2(c) shows the biplane model combined with slat and flap. The models were made of acrylic. The biplane element has a chord length c of 200 mm, a wing thickness t of 10 mm (t/c = 0.05), and a spacing between wing elements G of 100 mm (G/c = 0.5). The dimensions of the baseline configuration were calculated at a design Mach number of 1.7 [1], [2].

The position where the flaps are deflected is 0.3c from the leading edge or trailing

edge. The deflections of the leading-edge slat are δ_n = 0° and 15°. The deflection of trailing-edge flaps is δ_f = 30°. Previous studies have demonstrated that a 30° trailing-edge flap and a 15° leading-edge slat significantly improve the aerodynamic performance of the Busemann biplane airfoil [9], [10], [12], [13]. This study focuses on the aerodynamic interference phenomena of the biplane models. The detailed test cases will be described in experimental conditions.

2.3. Experimental conditions

In the experiments, the flow velocity is 15 m/s. Based on the wing chord length c = 200 mm, the Reynolds number Re is 2.1×10^5. The angle of attack varied from -10° to 30°. The detailed measurement conditions have been described in previous studies [11].

To compare with the performance of the biplane configuration, the tests of a single configuration of upper and lower elements are conducted. For the biplane model, the upper and lower elements were measured separately. The experiments utilized two flap deflection settings: a trailing-edge flap configuration (δ_n = 0°, δ_f = 30°) and a slat and flap configuration (δ_n = 15°, δ_f = 30°).

The total aerodynamic coefficients of the biplane model are defined by the sum of the elements in biplane configuration, as following equations:

$$C_{l(biplane\_total)} = C_{l(biplane\_upper)} + C_{l(biplane\_lower)} \tag{1}$$

$$C_{d(biplane\_total)} = C_{d(biplane\_upper)} + C_{d(biplane\_lower)} \tag{2}$$

where $C_{l\ (biplane\_total)}$ and $C_{d\ (biplane\_total)}$ are the total lift and drag coefficients of the biplane model. In biplane configuration, $C_{l\ (biplane\_upper)}$ and $C_{d\ (biplane\_\ upper)}$ are the lift and drag coefficients of the upper wing, and $C_{l\ (biplane\_\ lower)}$ and $C_{d\ (biplane\_lower)}$ are the lift and drag coefficients of the lower wing, respectively.

The aerodynamic interference ratio for a biplane is the ratio of its total lift and drag coefficients to the sum of the lift and drag coefficients of the individual upper and lower wings, measured as single-wing models [11]. The specific formula for its calculation is:

$$I_l = \frac{C_{l(single\_upper)} + C_{l(single\_lower)}}{C_{l(biplane\_total)}} \tag{3}$$

$$I_d = \frac{C_{d(single\_upper)} + C_{d(single\_lower)}}{C_{d(biplane\_total)}} \tag{4}$$

where $C_{l\ (single\_upper)}$ and $C_{d\ (single\_\ upper)}$ are the respective lift and drag coefficients for the single upper element, $C_{l\ (single\_\ lower)}$ and $C_{d\ (single\_lower)}$ are the lift and drag coefficients for the single lower element, respectively.

2.4. Numerical simulations

To compare and validate the experimental results, RANS (Reynolds-averaged Navier-Stokes) simulations were conducted. The computational mesh was generated using Ansys ICEM-CFD software.

Figure 3 illustrates the computational domain and mesh around the biplane models. The simulation domain with a length × width of 45*c* × 40*c* was sized to capture all flow phenomena around the wing surface during angle of attack variations. Approximately 400 mesh elements were placed on the wing surface, with the *y*+ value at the wing surface designed to be approximately 1.0. Mesh independency and simulation accuracy were investigated in previous studies [11].

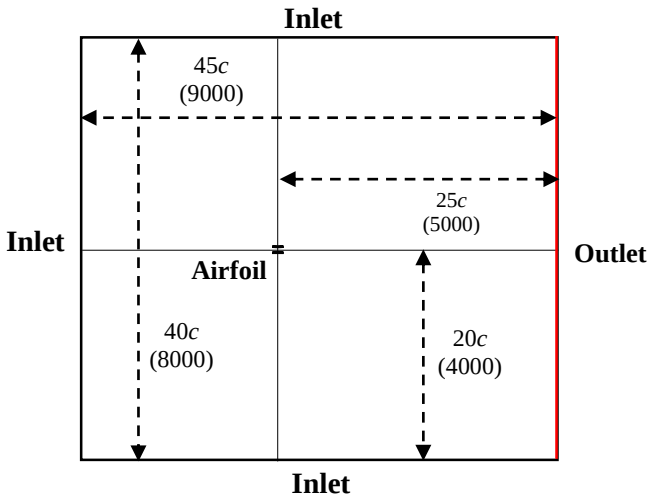

(a) Computational domain

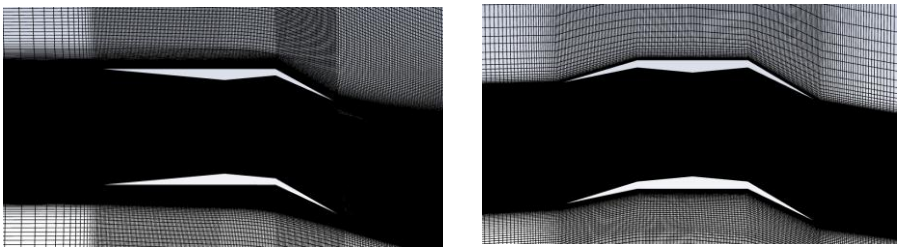

(b) Mesh distribution around the numerical models

Fig. 3. Meshs used for numerical simulations.

The simulations were performed using Ansys Fluent software, employing the Spalart-Allmaras (S-A) turbulence model and a coupled algorithm, as previous studies [11], [14], [15]. Convergence criteria for residuals and velocities were set to 10^{-6}. The computational boundary conditions were set to match the experimental conditions.

3. Results and discussions

3.1. Lift and drag coefficients

Figure 4 shows the lift coefficient for both the single and biplane models when equipped with trailing-edge flaps. The deflection of the flap is 30°.

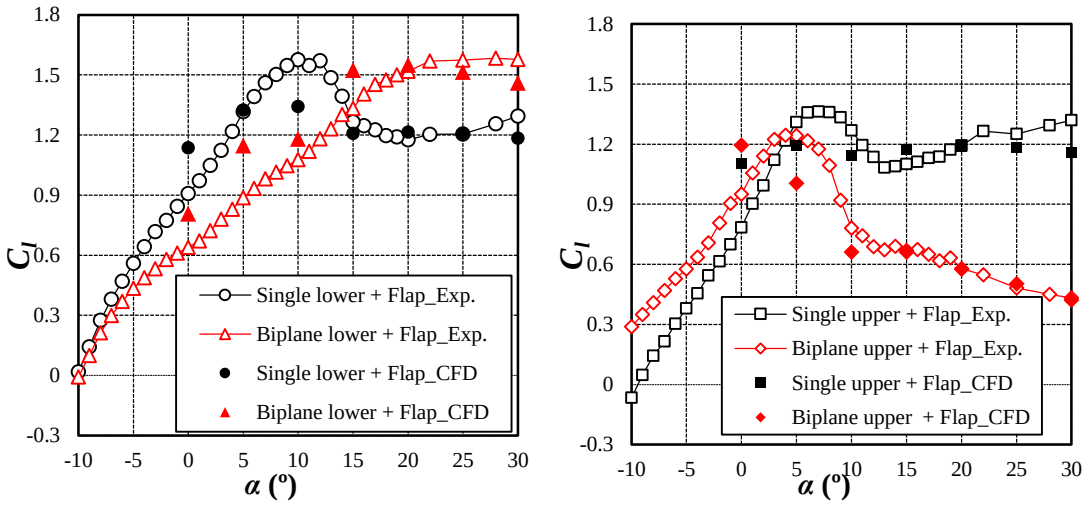

(a) Lower wing *(b) Upper wing*

Fig. 4. Lift coefficient of model with trailing edge flap.

In the single configuration with a trailing-edge flap, the lower wing generated more lift and less drag compared to the upper wing at angles of attack below 20°. The upper wing experienced stall at an 8° angle of attack, achieving a maximum lift coefficient of 1.36. In contrast, the lower wing reached a maximum lift of 1.57 at a 12° angle of attack, which was higher than the upper wing's maximum. For the biplane configuration with a trailing-edge flap, the lift coefficient $C_{l\ (biplane\ lower)}$ increased with the angle of attack. However, the lower wing produced less lift compared to its single configuration at angles of attack below 15° ($C_{l\ (biplane\ \ lower)} < C_{l\ (single\ \ lower)}$). The upper wing, conversely, stalled at an angle of attack of 5°, which is earlier than in the single-wing configuration.

Figure 5 shows the drag coefficient for both the single and biplane models when equipped with trailing-edge flaps. For a single wing with a flap, there's no significant difference in drag between the upper and lower wings. However, at angles of attack greater than 20°, the upper wing creates more drag than the lower wing. In the biplane configuration with a flap, the lower wing shows a minor increase in drag compared to the single configuration when the angle of attack is over 15°. Conversely, the drag coefficient of the upper wing stays almost constant and is much less than the single configuration when the angle of attack is above 7°.

Figure 6 presents the lift coefficient results for both the single-wing and biplane models when equipped with both leading-edge slats and trailing-edge flaps. The deflection of the leading-edge slat is $\delta_n = 15°$, and the deflection of the trailing-edge flap is $\delta_f = 30°$.

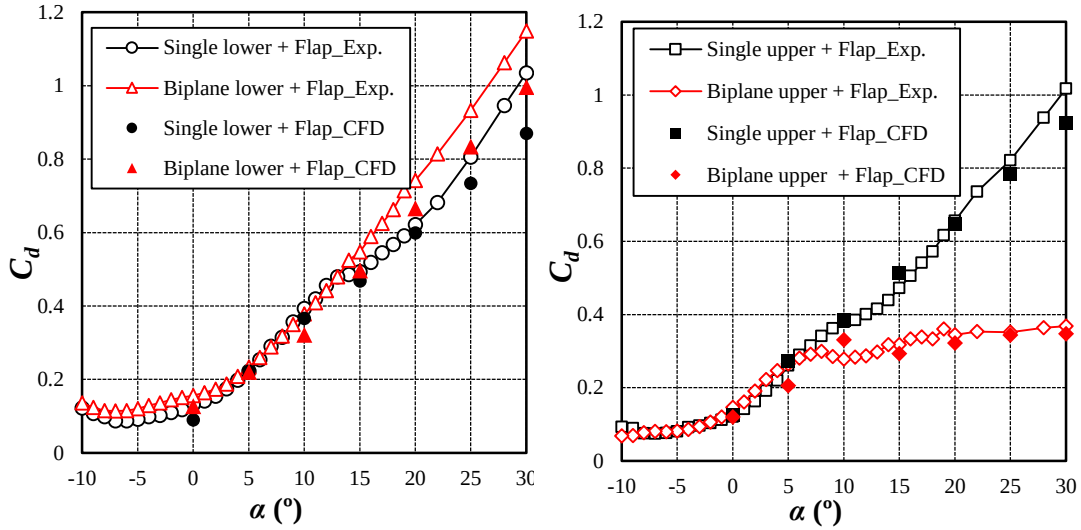

(a) Lower wing *(b) Upper wing*

Fig. 5. Drag coefficient of model with trailing edge flap.

When the angles of attack exceeded 10° in the single configuration, the lower wing produced more lift than the upper wing. The upper wing stalled at a 10° angle of attack, reaching a maximum lift coefficient of 1.53. In contrast, the lower wing achieved a higher maximum lift of 1.65 at a 13° angle of attack. These results show a similar trend to the single configuration with only trailing-edge flaps, as seen in Fig. 4. However, with the addition of a leading-edge slat, both the upper and lower single wings experienced stalling at a larger angle of attack and achieved a higher maximum lift compared to having only trailing-edge flaps. In the biplane configuration with slat and flap, the lower wing did not experience stall, and its lift coefficient increased with the angle of attack, similar to the case with only trailing-edge flaps. Nevertheless, the lower wing produced less lift compared to its single-wing counterpart at angles of attack below 20°. The upper wing stalled at a 10° angle of attack, which is consistent with its behavior in the single configuration. This result differs from the trend observed with only trailing-edge flaps, where the upper wing of the biplane stalled earlier than in the single-wing configuration.

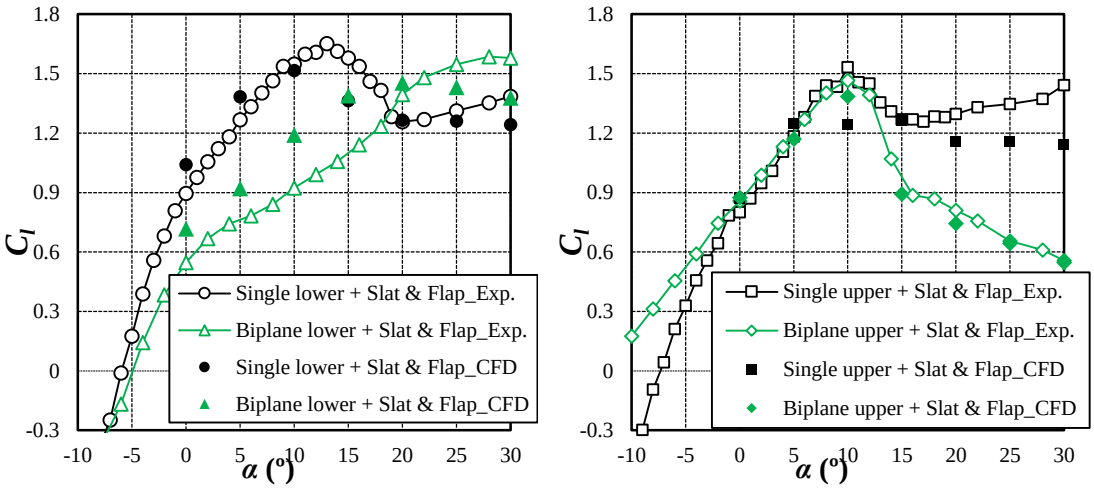

(a) Lower wing *(b) Upper wing*

Fig. 6. Lift coefficient of model with slat and flap.

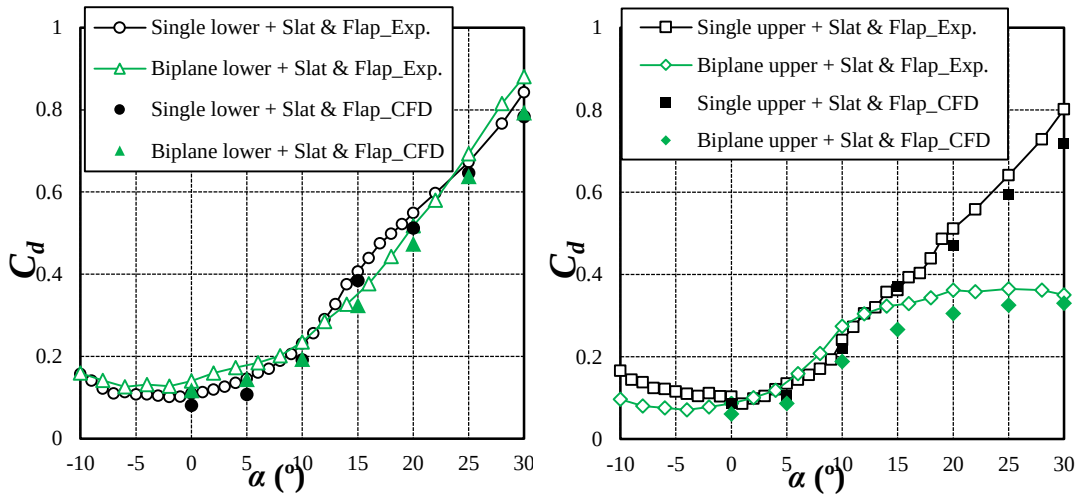

(a) Lower wing *(b) Upper wing*

Fig. 7. Drag coefficient of model with slats and flaps.

Figure 7 shows the drag coefficient results for both the single-wing and biplane models when equipped with both leading-edge slats and trailing-edge flaps. In the single configuration, no significant difference in drag coefficient was observed between the upper and lower wings. For the biplane configuration, the drag coefficient of the lower wing showed only a minor deviation when compared to its single configuration performance. Notably, at angles of attack exceeding 9°, the drag generated by the upper wing remained nearly constant and was considerably lower than that observed in the

single configuration. This trend aligns with observations from configurations utilizing only trailing-edge flaps.

The simulation results showed a deviation from the experimental data, which became more pronounced as the angle of attack increased. This discrepancy is likely due to the large vortices and strong interactions between the wings created by the leading-edge slat and trailing-edge flap. Similar to findings on the Stagger model [11], [12], these complex flow features present a challenge for computational models to accurately simulate. Despite this, the overall trends of the simulation and experimental data are in good agreement.

3.2. Aerodynamic interference ratio

Figure 8 shows the aerodynamic interference ratios for the biplane when equipped with slat and flap. The ratios were calculated using Eqs. (3) and (4). The aerodynamic interference ratios for the baseline biplane from previous research are included [11]. The aerodynamic interference ratio for a biplane wing indicates the interaction between the upper and lower elements, which alters the lift and drag compared to individual elements in a single configuration.

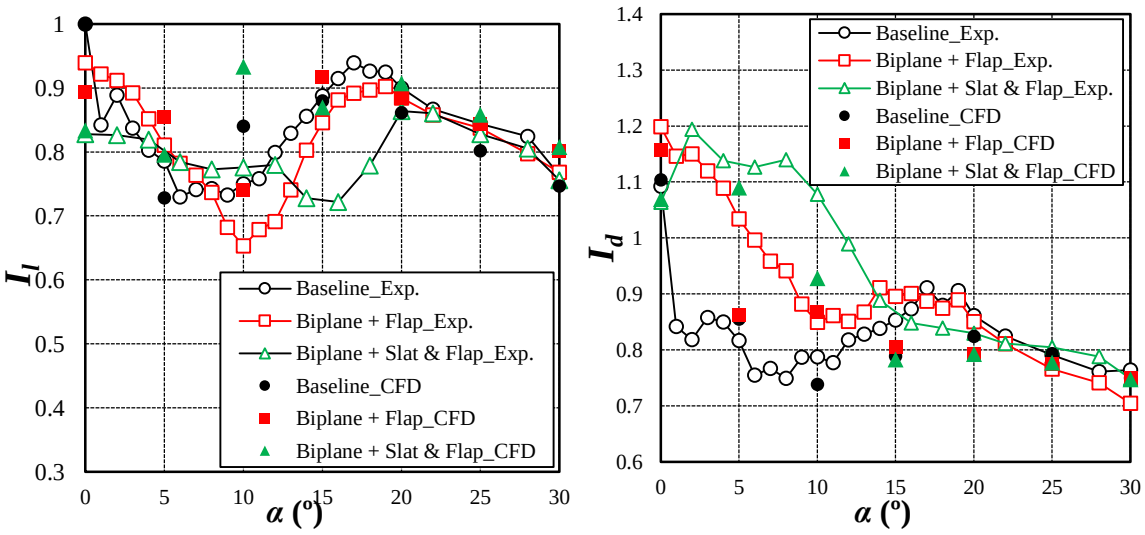

(a) Lift interference ratio *(b) Drag interference ratio*

Fig. 8. Aerodynamic interference ratio of biplane with slat and flap.

Figure 8(a) shows the lift interference ratio (I_l). For the biplane with trailing-edge flap, I_l varies between 0.65 and 0.9. I_l gradually decreases from 0° to 10° angle of attack, reaching its minimum of 0.65 at 10°. Compared to the baseline model, I_l shows a similar trend in its variation. However, the baseline model reaches a minimum of I_l at a 6° angle of attack with a value of 0.74. For the biplane with slat and flap, I_l gradually decreases

from 0° to 16° angle of attack, reaching its minimum of 0.72 at 16°. The leading-edge slat mitigates flow separation, allowing the Busemann airfoil to maintain lift at higher angles of attack than without a slat. For the Busemann biplane, the use of leading-edge slats on both wings significantly increases the total lift coefficient at angles of attack over 10°, as noted in previous studies [12], [13]. At high angles of attack, the leading-edge slat can reduce the separation regions, thereby limiting negative interactions between the flows on both wings and increasing the lift interference ratio.

Figure 8(b) shows the drag interference ratio (I_d). For the biplane with trailing-edge flap, I_d is greater than 1.0 at angles of attack smaller than 5°, indicating that the biplane configuration generates more drag compared to the total of the single configurations. For angles of attack between 10° and 20°, I_d varies between 0.85 and 0.9. Compared to the baseline model, the biplane with trailing-edge flap shows a similar trend in I_d variation. For the biplane with leading-edge slat and trailing-edge flap, I_d exceeds 1.0 at angles of attack smaller than 12°. The deployment of the leading-edge slat enhances the wing's camber, which is a significant contributor to the increased total drag of the biplane at low angles of attack. The slat functions by redirecting the incoming flow, which intensifies the low-pressure zones on the wing's upper surface. This effect leads directly to a rise in interference drag. Consequently, the drag interference ratio of the Busemann biplane tends to increase due to the complex flow interactions.

3.3. Pressure distribution around the models

Figure 9 illustrates the pressure distribution around the models equipped with a trailing-edge flap at angles of attack of 10° and 20°. A notable difference in pressure distribution is observed on the upper surface of the lower wing and the lower surface of the upper wing compared to their single-element counterparts. This disparity is attributed to the accelerated flow between the upper and lower elements within the biplane configuration. Furthermore, the biplane arrangement diminishes the high-pressure region typically found near the leading edge of the upper wing in a single configuration. This observation supports the results presented in Fig. 4, which indicated that a single upper wing generates greater lift and drag compared to the upper wing within the biplane configuration. Additionally, the characteristic low-pressure region observed in the single configuration is mitigated in the biplane configuration.

Figure 10 illustrates the pressure distribution around the models equipped with both slats and flaps. The angles of attack are 10° and 20°. In the single configuration, no significant difference in pressure distribution was observed between the upper and lower elements. However, the biplane configuration significantly reduces the high-pressure region beneath the upper wing compared to the single configuration. This observation supports the results presented in Fig. 6, where the lift generated by the upper element in

the biplane configuration was significantly smaller than in the single configuration. Furthermore, when compared to a biplane equipped only with a trailing-edge flap, the presence of the leading-edge slat mitigates the high-pressure region near the leading edge of the upper element.

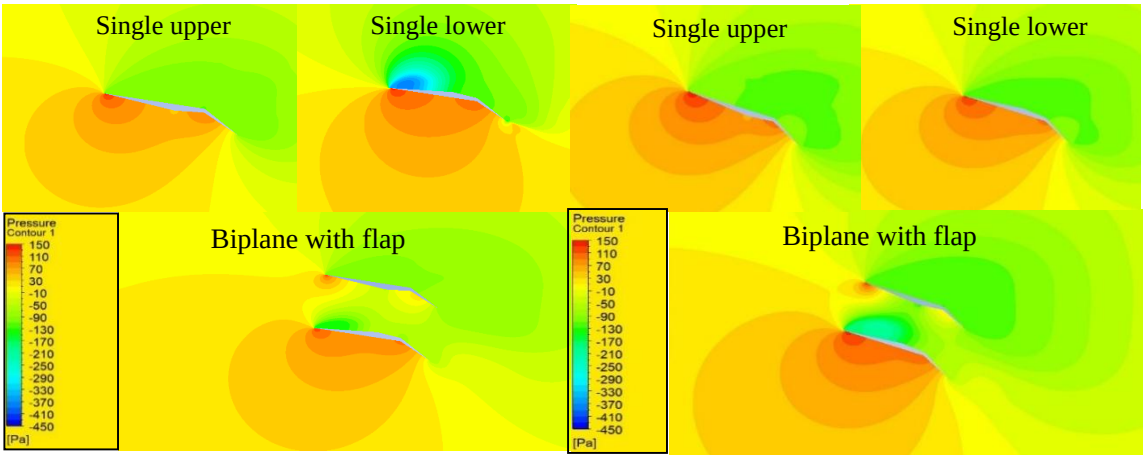

(a) α = 10° *(b) α = 20°*

Fig. 9. Pressure distributions around the bipalne with trailing-edge flap.

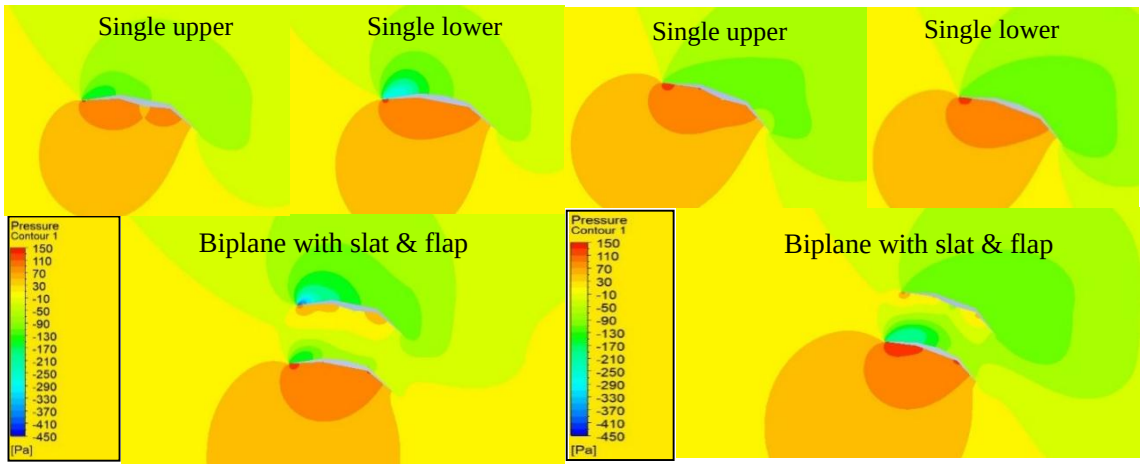

(a) α = 10° *(b) α = 20°*

Fig. 10. Pressure distributions around the bipalne with slat and flap.

4. Conclusion

In this study, the aerodynamic interference characteristics of a Busemann biplane airfoil incorporating both leading-edge slats and trailing-edge flaps are investigated by using wind tunnel experiments and numerical simulations.

Regarding the single-wing configuration equipped with a trailing-edge flap, stall

occurred on both the upper and lower wings in the single configuration. When both a leading-edge slat and a trailing-edge flap were present on the single wing, the addition of the slat enabled the single model to stall at a larger angle of attack, consequently leading to a higher maximum lift coefficient.

Considering the biplane configuration with slat and flap, the lower wing did not experience stall, and its lift coefficient increased with the angle of attack, similar to the case with only trailing-edge flaps. The drag generated by the upper wing remained nearly constant and was considerably lower than that observed in the single configuration at angles of attack exceeding 9°. This trend aligns with observations of configurations utilizing only trailing-edge flaps.

The aerodynamic interference ratio for the biplane configurations offers information about the interaction between the upper and lower elements. For the biplane with a trailing-edge flap, the drag interference ratio exceeded 1.0 at angles of attack below 5°. The lift interference ratio ranged from 0.65 to 0.9, reaching its minimum value at a 10° angle of attack. For the biplane configuration with both a slat and a flap, the drag interference ratio exceeded 1.0 at angles of attack below 12°. The lift interference ratio exhibited a minimum value of 0.72 at 16°.

The simulation results exhibited excellent agreement in trends with the experimental findings.

Acknowledgement

The authors would like to thank Professor Masashi Kashitani, Department of Aerospace Engineering of National Defense Academy of Japan for his support in the wind tunnel experiments.

References

[1] K. Kusunose *et al.*, "Aerodynamic design of supersonic biplane, cutting edge and related topics", The 21st Century COE Program, in International COE of Flow Dynamic Lecture Series, Sendai: Tohoku University Press, 2007.

[2] K. Kusunose, K. Matsushima, and D. Maruyama, "Supersonic biplane - A review", *Progress in Aerospace Sciences*, Vol. 47, pp. 53-87, 2011. DOI: 10.1016/j.paerosci.2010.09.003

[3] N. Kuratani, T. Ogawa, H. Yamashita, M. Yonezawa, and S. Obayashi, "Experimental and computational fluid dynamic around supersonic biplane for sonic boom reduction", *AIAA* 2007-3674, 2007. DOI: 10.2514/6.2007-3674

[4] H. Nagai, S. Oyama, T. Ogawa, N. Kuratani, and K. Asai, "Experimental study on interference flow of a supersonic Busemann biplane using pressure-sensitive paint technique", The 26th International Congress of the Aeronautical Sciences, 2008.

[5] Y. Odaka and K. Kusunose, "A fundamental study for aerodynamic characteristics of supersonic biplane wing and wing-body configurations", *Journal of the Japan Society for Aeronautical and Space Sciences*, Vol. 57, pp. 217-224, 2009 (in Japanese). DOI: 10.2322/jjsass.57.217

[6] W. Yamazaki and K. Kusunose, "Biplane-wing/Twin-body-fuselage configuration for innovative supersonic transport", *Journal of Aircraft*, Vol. 51, No. 6, pp. 1942-1952, 2014. DOI: 10.2514/1.C032581

[7] T. D. Nguyen *et al.*, "Analysis of a Wing-Fuselage Biplane with Trailing-Edge Flaps in Low-Speed Flow", *Journal of Aircraft*, Vol. 59, No. 2, pp. 350-363, 2021. DOI: 10.2514/1.C036154

[8] H. Yamashita, S. Obayashi, and K. Kusunose, "Reduction of drag penalty by means of plain flaps in the boomless Busemann biplane", *International Journal of Emerging Multidisciplinary Fluid Sciences*, Vol. 1, pp. 141-164, 2009. DOI: 10.1260/175683109788707490

[9] D. Maruyama, K. Kusunose, K. Matsushima, and K. Nakahashi, "Aerodynamic analysis and design of Busemann biplane: Towards efficient supersonic flight", in *Proceedings of the Institution of Mechanical Engineers, Part G: Journal of Aerospace Engineering*, Vol. 226, Iss. 2, pp. 217-238, 2012. DOI: 10.1177/09544100114046

[10] M. Kashitani, T. D. Nguyen, M. Taguchi, and K. Kusunose, "Aerodynamic characteristics of Busemann biplane installed with high-lift device using low-speed smoke wind tunnel", *AIAA SciTech 2022*, America, AIAA 2022-0140, 2022. DOI: 10.2514/6.2022-0140

[11] T. D. Nguyen, M. Kashitani, M. Taguchi, and K. Kusunose, "Effects of stagger on low-speed performance of Busemann biplane airfoil", *Aerospace*, Vol. 9, No. 197, pp. 1-23, 2022. DOI: 10.3390/aerospace9040197

[12] N. T. Dương và T. H. Hùng, "Nghiên cứu đặc tính khí động cánh hai tầng dạng Busemann có cánh tà tại vận tốc dưới âm", *Journal of Science and Technique*, Vol. 20, No. 1, tr. 53-67, 2025. DOI: 10.56651/lqdtu.jst.v20.n01.895

[13] T. D Nguyen, M. Kashitani, M. Taguchi, and K. Kusunose, "Analysis of low-speed aerodynamic characteristics of Busemann biplane airfoil installed high lift devices", 33rd Congress of the International Council of the Aeronautical Sciences (33rd ICAS), Sweden, ICAS-0145, 2022.

[14] P. R. Spalart and C. L. Rumsey, "Effective inflow conditions for turbulence models in aerodynamics calculations", *AIAA Journal*, Vol. 45, pp. 2544-2553, 2007. DOI: 10.2514/1.29373

[15] Y. Cai, G. Liu, W. Zhu, Q. Tu, and G. Hong, "Aerodynamic interference significance analysis of two-dimensional front wing and rear wing airfoils with stagger and gap variations", *Journal of Aerospace Engineering*, Vol. 32, Iss. 6, 2019. DOI: 10.1061/(ASCE)AS.1943-5525.0001090.

ĐẶC ĐIỂM GIAO THOA KHÍ ĐỘNG CỦA CÁNH HAI TẦNG BUSEMANN CÓ CÁNH CẢN VÀ CÁNH TÀ Ở TỐC ĐỘ THẤP

Nguyễn Thái Dương[1], Phạm Quang Huy[2], Trần Thế Hùng[3]

[1]*Trung tâm Hợp tác quốc tế Khoa học công nghệ Việt-Nhật, Trường Đại học Kỹ thuật Lê Quý Đôn*

[2]*Trung tâm Khí cụ bay, Tổng công ty Công nghiệp công nghệ cao Viettel*

[3]*Khoa Hàng không Vũ trụ, Trường Đại học Kỹ thuật Lê Quý Đôn*

Tóm tắt: Nghiên cứu này tập trung làm rõ đặc điểm giao thoa khí động của cánh hai tầng Busemann khi có cánh cản và cánh tà trong dòng chảy tốc độ thấp bằng các thực nghiệm trong hệ thống ống thổi khí động và mô phỏng số. Đặc tính khí động học của cấu hình hai tầng cánh được phân tích so sánh với hiệu suất của cánh trên và cánh dưới khi ở cấu hình một cánh đơn. Góc gập của cánh cản và cánh tà tương ứng là là 15° và 30°. Trong cấu hình cánh đơn, hiện tượng thất tốc xuất hiện ở cả cánh trên và cánh dưới. Cánh cản ở mép trước làm góc tấn thất tốc lớn hơn và hệ số lực nâng cực đại cao hơn so với cấu hình cánh đơn chỉ có cánh tà. Trong cấu hình cánh hai tầng, cánh dưới không bị thất tốc, và hệ số lực nâng của cánh dưới tăng dần theo góc tấn trong tất cả các trường hợp. Hệ số giao thoa lực cản vượt quá 1,0 ở các góc tấn dưới 5° với cấu hình cánh hai tầng chỉ có cánh tà ở mép sau, và ở các góc tấn dưới 12° đối với cấu hình có cả cánh cản và cánh tà. Hệ số giao thoa lực cản lớn hơn 1,0 cho thấy rằng trong khoảng này, cấu hình hai tầng cánh tạo ra tổng lực cản lớn hơn tổng lực cản của từng cánh riêng lẻ ở cấu hình cánh đơn. Hệ số giao thoa lực nâng đạt giá trị nhỏ nhất là 0,72 tại góc tấn 16° với cánh hai tầng có cánh cản và cánh tà.

Từ khóa: *Cánh hai tầng Busemann; cánh cản; cánh tà; hệ số giao thoa khí động.*

Received: 26/06/2025; Revised: 02/10/2025; Accepted for publication: 27/01/2026

❑